Metamorphosis of plasma turbulence–shear-flow dynamics through a transcritical bifurcation

R. Ball* and R. L. Dewar
Department of Theoretical Physics, Research School of Physical Sciences and Engineering, The Australian National University, Canberra ACT 0200, Australia

H. Sugama
National Institute For Fusion Science, Oroshi-cho, Toki GIFU 509-5292, Japan
(Received 21 June 2002; published 16 December 2002)

The structural properties of an economical model for a confined plasma turbulence governor are investigated through bifurcation and stability analyses. A close relationship is demonstrated between the underlying bifurcation framework of the model and typical behavior associated with low- to high-confinement transitions such as shear-flow stabilization of turbulence and oscillatory collective action. In particular, the analysis evinces two types of discontinuous transition that are qualitatively distinct. One involves classical hysteresis, governed by viscous dissipation. The other is intrinsically oscillatory and nonhysteretic, and thus provides a model for the so-called dithering transitions that are frequently observed. This metamorphosis, or transformation, of the system dynamics is an important late side-effect of symmetry breaking, which manifests as an unusual nonsymmetric transcritical bifurcation induced by a significant shear-flow drive.

DOI: 10.1103/PhysRevE.66.066408 PACS number(s): 52.30.−q, 52.25.Xz, 05.45.−a, 52.35.Ra

I. INTRODUCTION

Fusion plasmas, and possibly other quasi-two-dimensional fluid systems, may undergo a more-or-less dramatic transition from a low- to a high-confinement state (the *L*-*H* transition) as the power input is increased, with the desirable outcome that particle and energy confinement is greatly improved due to localized transport reduction [1]. In this work we report on a bifurcation and stability probe of an economical model for *L*-*H* transition dynamics that uncovers a mechanism by which a radical change, or metamorphosis, may occur in the qualitative nature of the dynamics. We apply the results of this analysis to clarify the relationship between the structure of the model and the physics of the process that it describes, and draw comparisons with characteristics of *L*-*H* transitions observed in various experiments.

Since 1988 there has been much progress in developing low-dimensional (low-order or reduced) descriptions of *L*-*H* transition dynamics and associated oscillatory phenomena (see, for example, Refs. [2–15]), the driving force being the potential power of a unified, low-dimensional model as a predictive tool for the design and control of confinement states. For example, a model that speaks of the shape and extent of hysteresis in the *L*-*H* transition would help engineers who are interested in controlling access to H mode. Given the many variables and parameters that *could* be varied around a hysteretic regime, it would be cheaper—i.e., save hundreds of CPU hours and (or) many expensive diagnostics—to know in advance which ones actually *do* affect the hysteresis, and which do not.

To help construe the context in which low-dimensional descriptions of plasma dynamics are sought, it is appropriate at this stage to make some general remarks. It makes sense to try to find the simplest description of an evolving system that is consistent with the time and space scales on which one is interested in making experimental observations of that system. One would like the description to incorporate the qualitative nature of the system structure and dynamics, so that it can be used for design and control purposes and make useful predictions. A truly useful description usually turns out to be a low-dimensional system of coupled ordinary differential equations. Such descriptions are powerful because they are supported by well-developed theories that give qualitative and global insight, such as bifurcation, stability, and symmetry theory [16,17]. In principle, we can map analytically the bifurcation structure of the entire state and parameter space of a low-dimensional dynamical system, but this is not possible for an infinite-dimensional system and not practicable for systems of high order.

However, the quest for a low-dimensional state space that captures the qualitative dynamics of *L*-*H* transitions has been problematic. It has been shown [18,15] that some of the models cited above do not reflect salient features of *L*-*H* transitions such as shear-flow suppression of turbulence, or are incomplete, or show profound structural discrepancies, although it is intuitively reasonable to expect that manifestly different models should be equivalent at some deeper level if they describe the same phenomena.

By economical, or minimal, model we mean the smallest, functionally simplest, and mathematically consistent model that captures qualitatively the dynamical traits that are typically observed over many experiments in different machines. The strength and potency of a minimal model is just this universality; its apparent disregard for details, numbers and unit dimensions is sometimes perceived—wrongly—as a weakness. In keeping with this ideology we introduce here a consensus dynamical model that is economical in terms of variables and parameters, and incorporates the smallest number of rate processes of simplest functional form needed to reflect the universally observed dynamics. If the model is

*Electronic address: Rowena.Ball@anu.edu.au

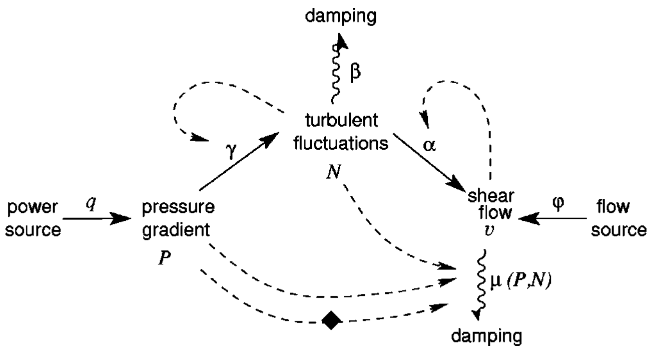

FIG. 1. A plasma turbulence governor, showing the coupled rates and feedback processes that contribute to the dynamics of L-H transitions. Solid arrows indicate generation rates, wavy arrows dissipation, dashed arrows feedback on rate coefficients; the black diamond indicates negative feedback.

successful we expect additional terms to have only quantitative, not qualitative or structural, effects. We should also be able to identify easily its limits of validity, or where it breaks down and why.

In Sec. II we introduce the plasma turbulence governor as a useful schema to conceptualize and represent the major contributing rate and feedback processes, relating these to the corresponding dynamical system. Bifurcation and stability analyses and interpretive discussions, with reference to reported experiments, are given in the remaining sections. In Sec. III we begin by determining the two highest-order (most degenerate) singularities in the system, or *organizing centers*. Section IV describes the generic bifurcation diagram and discusses the hysteresis and limit cycles in the system. In Sec. V we illustrate and discuss the useful properties of the two-parameter bifurcation diagram. This discussion leads in to Sec. VI, in which we determine explicitly the transcritical metamorphosis to an oscillatory, nonhysteretic regime. A short summary is given in Sec. VII. The Appendix contains a derivation of the dynamical equations.

II. COMPETITIVE AND FEEDBACK PROCESSES GOVERN PLASMA TURBULENCE

The schematic in Fig. 1 is a primitive of a plasma turbulence governor. (The name is intended to refer to archetypical mechanical exemplars of feedback controllers such as James Watt's 1788 steam-engine governor. In Ref. [19] a comparable scheme was called the "barotropic governor," in the context of quasi-two-dimensional atmospheric flows.) A power input q creates a pressure gradient P from which the turbulent density fluctuation intensity N grows at a rate with coefficient γ. The turbulence feeds energy into the poloidal shear flow v via the Reynolds stress α. The shear flow is generated externally at rate φ and damped by the ion viscosity μ. The turbulence is damped quadratically with coefficient β. Also indicated is a *competitive* distribution of energy from the pressure gradient, whereby different fractions may partition into turbulence generation and shear-flow damping. It is not difficult to appreciate how the various rate and competitive processes in Fig. 1 could balance out—or rather, *un*balance out—so as to give rise to the oscillatory and hysteretic dynamics that are characteristic of L-H transitions.

The reduced dynamical system that models this scheme is based on the Sugama-Horton model [7], which itself was derived from approximate resistive magnetohydrodynamics (MHD) vorticity and pressure convection equations [20,21],

$$\varepsilon\frac{dP}{dt}=q-\gamma PN, \tag{1}$$

$$\frac{dN}{dt}=\gamma PN-\alpha v^2N-\beta N^2, \tag{2}$$

$$2\frac{dv}{dt}=\alpha vN-\mu(P,N)v+\varphi, \tag{3}$$

$$\mu(P,N)=bP^m+aP^rN. \tag{4}$$

In terms of the shear-flow kinetic energy $F=v^2$, Eqs. (2) and (3) may be written as

$$\frac{dN}{dt}=\gamma PN-\alpha FN-\beta N^2, \tag{2$'$}$$

$$\frac{dF}{dt}=\alpha FN-\mu(P,N)F+\varphi F^{1/2}. \tag{3$'$}$$

The derivation of this system is given in the Appendix. The most important modification to the original Sugama-Horton model is the symmetry-breaking term φ in Eq. (3). It will be seen that this term, which may be interpreted as an external shear-flow driving rate, has dramatic effects on the bifurcation structure of the system.

The first and second terms in the bipartite viscosity function, Eq. (4), model the neoclassical and anomalous viscosity damping, respectively. In a plasma of low collisionality the exponent m is negative so a high pressure gradient has the effect of blocking the neoclassical contribution. (Refer to Fig. 1.) Under these circumstances energy can accumulate in the shear flow then feed back into turbulence decorrelation. On the other hand, a high pressure gradient and high turbulence levels both *enhance* the anomalous viscosity damping, because the exponent r is positive. The net effect will depend on the relativity of the three competitive rates involved in the distribution of energy from the pressure gradient.

III. PITCHFORK P^* AND DULL BIFUCATION D^* ARE LOCAL HIGHEST-ORDER SINGULARITIES

Generally in bifurcation analysis we are interested in the multiplicity, stability, singularity, and parameter dependence of zero solutions of a bifurcation equation $g=G(x,\lambda_1,\lambda_2,\ldots,\lambda_n)$, where x is a state variable and the λ_i are parameters, that is derivable (in principle if not always in practice) from the equilibria of a dynamical system.

In Eqs. (1)–(4) we may select $x\equiv P$ and the principal bifurcation parameter $\lambda_1\equiv q$ and set the right hand sides to zero to obtain the bifurcation equation,

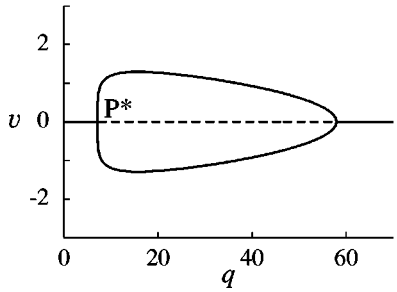

FIG. 2. Bifurcation diagram for the critical set (P*), $\varphi=0$, $b=18.58$, $\alpha=2.4$, $\beta=1$, $\gamma=1$, $a=0.3$, $\varepsilon=1.5$.

$$g=\frac{1}{2P^2\alpha\gamma^2}(aP^r q-q\alpha+bP^{1+m}\gamma)(q\beta-P^2\gamma^2)+\frac{\varphi(P^2\gamma^2-q\beta)^{1/2}}{2(P\alpha\gamma)^{1/2}} \tag{5}$$

[where Eq. (3′) has been used]. Singular points occur where $g=g_P=0$. (Subscripts on g denote partial derivatives with respect to the subscripted variable.) On the $v=0$ curve they are given by

$$(P,q,\varphi)=(P_i,P_i^2\gamma^2/\beta,0),$$

with the P_i given by the real, positive roots of $\beta b+P^{1-m}(aP^r-\alpha)\gamma=0$. At these points $g_q=0$ and $g_{PP}=-8[aP_i^r(-1-m+r)+(1+m)\alpha]\gamma^2/(\alpha\beta)$. Thus for some values of the exponents m and r one or more of the singularities may comply with the pitchfork conditions

$$g=g_P=g_q=0=g_{PP}=0,\ \ g_{PPP}\neq 0,\ \ g_{Pq}\neq 0. \tag{6}$$

Obviously (since g_{PP} must equal 0), compliance with these conditions also implies the existence of hysteresis.

To specify the dependence of the viscosity damping on the pressure gradient in Eq. (4) we set $m=-3/2$ and $r=1$, as in Ref. [7]. This value of m applies for the temperature dependence of the ion viscosity in a low collisional regime [22]. The value of $r=1$ is the simplest that is consistent with the suggested dependence of the anomalous viscosity on the ion temperature in Ref. [23].

With this specification the conditions in Eq. (8) applied to Eq. (7) find the unique pitchfork P* as

$$(v,q,b,\varphi)=\left(0,\frac{\alpha^2\gamma^2}{9a^2\beta},\frac{2\alpha^3\gamma\sqrt{\alpha/a}}{27\sqrt{3}a^2\beta},0\right). \tag{P*}$$

At P* the two nondegeneracy conditions in Eq. (8) evaluate as $g_{Pq}=8a/\alpha$, $g_{PPP}=-18a\gamma^2/(\alpha\beta)$. A pitchfork is described as a codimension-2 singularity, because its universal unfolding requires two parameters additional to the principal bifurcation parameter. Note that the second unfolding parameter, chosen here as b, can be any of the dissipative parameters a, b, or β. For reference the bifurcation diagram in Fig. 2 has been computed and plotted for the critical set (P*).

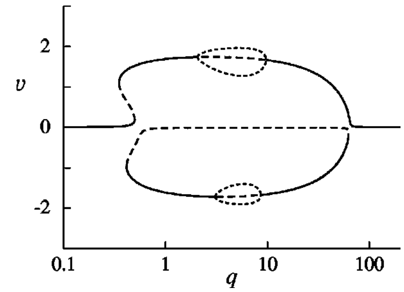

FIG. 3. Bifurcation diagram with $b=1$, $\varphi=0.02$, other parameters as for Fig. 2.

The singular point on the $v=0$ curve at high q complies with the conditions

$$g=g_P=g_q=0,\quad g_{PP}\neq 0,\quad \det d^2g<0, \tag{7}$$

where d^2g is the Hessian matrix of second partial derivatives $(g_{PP_{g_{qP}}} g_{qP_{g_{qq}}})$. A singular point that satisfies these conditions is usually termed as a transcritical bifurcation, or sometimes a "simple bifurcation."

For noncritical values of b (i.e., $b\neq b_{(\mathrm{P}*)}=18.58\ldots$), P* collapses to a second transcritical bifurcation on the $v=0$ curve. These two transcriticals coalesce and annihilate each other at a second codimension 2 singularity D* on the $v=0$ curve, defined by the conditions

$$g=g_P=g_q=\det d^2g=0,\quad g_{PP}\neq 0,\quad g_{Pq}\neq 0, \tag{8}$$

and found using Eq. (7) as

$$(v,q,b,\varphi)=\left(0,\frac{(5\alpha\gamma)^2}{(7a)^2\beta},\frac{50\sqrt{5\alpha/(7a)}\,\alpha^3\gamma}{7^3a^2\beta},0\right), \tag{D*}$$

with $g_{PP}=-32\gamma^2/(7\beta)$, $g_{Pq}=16a/(5\alpha)$. The bifurcation diagram showing this point (at $(v,q,b,\varphi)=(0,0.61\ldots,53.52\ldots,0)$ for values of the other parameters as in Fig. 2) would be extremely dull and flat—it consists only of the line $v=0$. Such a highly dissipative system has no interesting behavior at all.

IV. WALK THE SOLUTION CURVES, TALK THE PHYSICS

A bifurcation diagram for noncritical values of the unfolding parameters b and φ is shown in Fig. 3. (In the bifurcation diagrams stable solution branches are indicated by solid lines, unstable branches by dashed lines, and the dotted lines trace out the maximum and minimum amplitude of limit cycle branches.) This figure is richly informative but not immediately transparent or intuitive, so we shall walk through it with the reader, pausing to discuss significant features.

A. Jumps can occur to positive or negative *H*-mode branches

Standing back from Fig. 3 first, overall we can see that the symmetry evident in Fig. 2 is now broken, by the selection of a small positive value of φ. This symmetry-breaking parameter determines a preferred direction of the poloidal shear

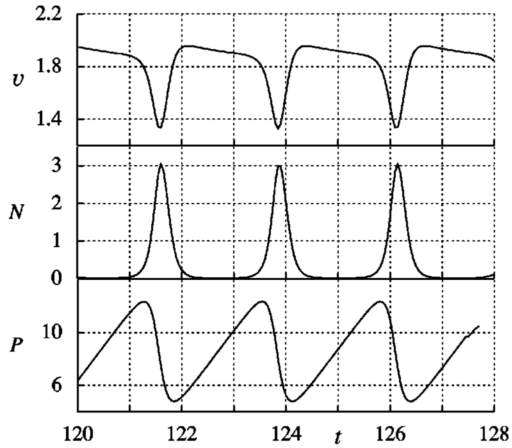

FIG. 4. A time series for $q=4$ on the $+v$ curve. Other parameters are the same as in Fig. 3.

flow. There are now two unconnected curves of solutions: a positive v curve and a negative v curve.

The $+v$ curve is plotted beginning at $q=0.1$ and $v \approx 0.004$. The stable solutions along the curve to the limit point s_L at $(v,q) \approx (0.2,0.495)$ comprise the L-mode branch, where the pressure gradient feeds the turbulence (refer to Fig. 5) and the anomalous viscosity damping, but does not inhibit the neoclassical viscosity damping enough to allow the shear flow to increase very much. At s_L the solutions become unstable and the system must jump to another stable attractor, which would normally be the stable solution at $(v,q) \approx (1.5,0.495)$. This section of the curve with high positive shear flow represents the $+v$ H-mode branch.

If the system is given a sufficiently strong, transient, opposing kick near s_L, it may also be forced onto the stable part of the $-v$ curve. This is the $-v$ H-mode branch, but because symmetry has been broken in favor of $+v$ solutions the shear flow is not as high. (For example, $-v \approx 1.3$ at $q = 0.495$.) Shear-flow reversal may also be forced from the $-v$ curve. On the other hand, reports of *spontaneous* reversals in the direction of main or impurity ion poloidal shear flow [32,33] can be rationalized from Fig. 3. In a system sitting on the $-v$ curve, the poloidal shear flow *must* reverse if a perturbation decreases the power input below that at the $(-v,q)$ limit point, s_{H^-}. Here the $+v$ curve provides the only stable attractors. Normally one would expect the system to move onto the L-mode branch, but an additional transient could take it to the H-mode branch of the $+v$ curve.

B. Passage through an oscillatory region

Continuing from left to right along the $+v$ and $-v$ H-mode branches (we are allowed to walk on two paths at once across this diagram) we arrive at at a point on each curve where the solutions again become unstable. These points are Hopf bifurcations, which occur when the Jacobian matrix of a linearised system of ODE has a pair of pure imaginary eigenvalues and no other eigenvalues with zero real part. As the bifurcation parameter passes through such a point a periodic orbit appears, encircling the equilibrium. (The finer details and technicalities of the Hopf bifurcation

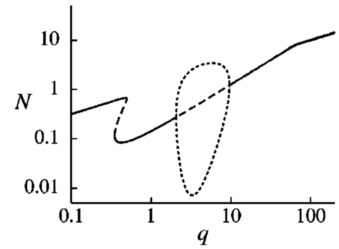

FIG. 5. Bifurcation diagram with N as a chosen state variable, showing the curve that corresponds to the $+v$ curve in Fig. 3.

are given in [16]. In this work the eigenvalues of Eqs. (1)–(3) were computed numerically.)

In Fig. 3 the first Hopf bifurcations h_A^+ and h_A^- occur at $(+v,q) \approx (1.74,2.06)$ and $(-v,q) \approx (1.72,3.06)$. Here the system must develop stable periodic behavior, because the branches of limit cycles that emanate from the Hopf bifurcations are stable while the equilibrium solutions are unstable.

Looking back along the $+v$ path traversed so far, the jump to the stable H-mode branch and subsequent appearance of limit cycles at h_A^+ reflect reports from experiments that a transition to a quiescent H mode can be achieved followed by the onset of oscillatory behavior, or edge-localized modes (ELM), as the power input continues to be increased [24–27].

Moving forward again we see the limit cycles growing in amplitude, as shown by the amplitude envelopes (dotted lines). The relative phases of v, N, and P are shown in the time series of Fig. 4. The original Sugama-Horton model was found to exhibit a chaotic time series for a particular set of parameter values in this regime [28]. In our model we have found that, under conditions of poor dissipation, the $+v$ branch of limit cycles can undergo several successive period doubling bifurcations followed by period halvings back to a period-one limit cycle.

At moderately high power input the pressure gradient and turbulence are high, neoclassical viscous damping is inhibited, and large amplitude oscillations would be expected as energy alternately accumulates in the shear flow and is exchanged with the turbulence. However, this is countered by the *enhancement* of *anomalous* viscosity damping by the larger amounts of turbulence and pressure gradient energy at higher power inputs. (Refer to the governor schematized in Fig. 1.) As this anomalous viscosity effect begins to take over after the amplitude maximum, the limit cycles shrink quite rapidly until at the second Hopf bifurcations h_B^+ and h_B^-, at $(+v,q) \approx (1.66,9.83)$ and $(-v,q) \approx (1.67,8.69)$, they are *extinguished*.

Although definitive experiments have not yet been performed that measure the growth and extent of the H-mode oscillations over the power input, it is physically reasonable that they would be limited by some damping factor. The passage through an oscillatory regime with increasing power is a characteristic of type-III ELMs [29,30]. However, the quantitative features of type-III ELMs, such as the frequency spectrum, are not reproduced by this simple model.

On the $-v$ curve the limit cycles are smaller in amplitude and occur over a smaller range of the power input. At

$q \approx 2.5$, for example, the $+v$ H mode is oscillatory but the $-vH$ mode is quiescent. Again, to our knowledge the appropriate experiments have not yet been carried out, but this is reminiscent of the prescription given in Ref. [31]: "The key factors in creating the quiescent *H*-mode operation are neutral beam injection in the direction opposite to the plasma current (counterinjection) plus cryopumping to reduce the density."

C. Further on and higher up

The shear flow reaches a broad maximum with increasing power input, then gradually decreases (note that the horizontal scale is logarithmic) to the the *L*-mode level. This would be reasonable behavior on physical grounds—one would not expect the shear flow to increase indefinitely with power input, because the turbulent viscosity damping (the second term in Eq. (4) with $r=1$) begins to take over as the power input pushes up the pressure gradient.

Clearly there is a scope for tuning other parameters in the model so as to obtain a complete picture of the steady states and limit cycles over parameter space, and more quantitative agreements with experiments. One may wish, for example, to maximize the range of q over which turbulence stabilization occurs, or minimize the range of q over which limit cycles occur, or both.

D. The way back

Figure 3 also shows the hysteresis predicted by compliance with the conditions in Eq. (8). Retracing our steps along the $+v$ curve we find that the back transition at the limit point s_{H^+} occurs at $q \approx 0.35$. Transitions with hysteresis have been observed in several machines: DIII-D [25], Asdex upgrade [34,35], JET, and in simulations of ITER [26], and Alcator C-mod [36]. Hysteresis is typically modified by dissipation, characterized in this model by the parameters β, b, and a. However, hysteresis does not seem to be a necessary or universal feature of discontinuous transitions.

One of the typical features of *L*-*H* transitions that a minimal model should reflect is suppression of the turbulence by the shear flow. Figure 5 shows the bifurcation diagram with the mean square turbulence level N as the state variable, where for clarity only the curve that matches the $+v$ curve is given. The turbulence is clearly suppressed over the hysteretic region, then begins to grow again as the higher pressure gradient from higher power input creates more turbulence.

V. CURVES OF SINGULAR POINTS HAVE MUNDANE MAXIMA AND INTERESTING MINIMA

The width and extent of hysteresis for selected values of b can be judged from the *two-parameter bifurcation diagram* for the $+v$ curve in Fig. 6, in which computed curves of the singular points in Fig. 3 are shown. The solid lines mark the loci of limit points (which are also sometimes called fold or saddle-node bifurcations) as b is varied. The dot-dash line is the locus of Hopf bifurcations as b is varied. If one can imagine taking slices across this diagram at various important values of b, the bifurcation story of the system can be told compactly, by inferring a reconstruction of the single-parameter (q,v) bifurcation diagram corresponding to each selected value of b.

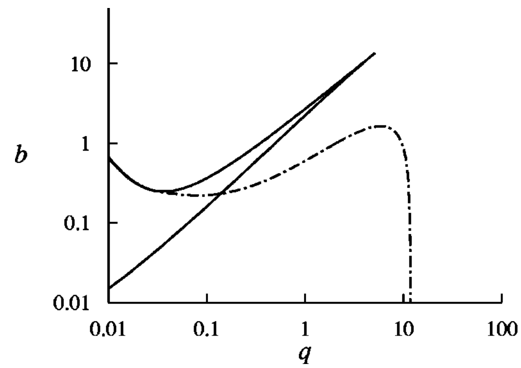

FIG. 6. Two-parameter curves of the singular points in Fig. 3. Solid lines are the loci of the limit points, dot-dash lines are the Hopf bifurcation loci.

A slice taken above the critical value of b at the cusp would yield a (q,v) bifurcation diagram that shows no multiplicity of states. Thus, in a highly dissipative system any transition is expected to be smooth and gradual rather than discontinuous, and a number of experiments suggest this conjecture. In ASDEX Upgrade the power hysteresis disappears at higher density (which implies more collisional damping) where gradual rather than discontinuous confinement improvement occurs [35]. A regime in which density fluctuation amplitudes are reduced continuously was also observed in Ref. [37]. In Ref. [38] a discontinuous bifurcation of the electric field in a stellarator was reported for conditions of low neutral density, where the charge-exchange damping rate is low. The change in the electric field became gradual for conditions of high neutral density, because the charge-exchange damping rate increases. (The electric field is related to the poloidal shear flow and the pressure gradient through the radial force balance [39].)

Oscillatory behavior is also expected to be damped out at high dissipation rates. The maximum in the locus of Hopf bifurcations in Fig. 6 occurs at the value of b, where the two Hopf bifurcations on the $+v$ curve in Fig. 3 annihilate each other (or conversely, are created). Above this value of b the $+v$ curve is stable with no associated limit cycles.

As slices are taken at lower b the hysteresis and the range of oscillatory behavior evidently become broader. At low dissipation rates the feedback is strong and nonlinear behavior is expected to be more pronounced.

The crossing of the Hopf and limit point loci in Fig. 6 is nonlocal, i.e., the value of P (and of v and N) at the crossing on the Hopf curve is different from that on the limit point curve. Within the overlapping region a direct transition to an oscillatory H mode may occur.

VI. THE METAMORPHOSIS

The minimum in the limit point curve of Fig. 6 implies the existence of another transcritical bifurcation [defined by Eq. (A2)] in the system, that occurs at nonzero v. This nonsymmetric transcritical bifurcation may have important is-

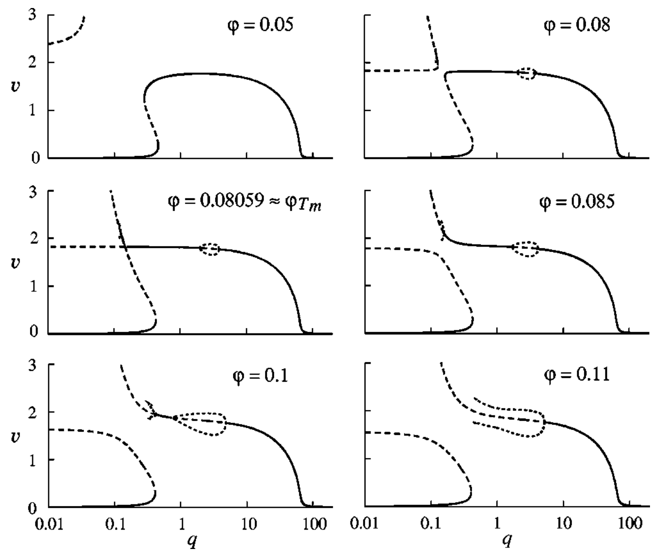

FIG. 7. A series of bifurcation diagram snapshots taken at increasing values of φ illustrates the exchange at φ_{T_m} and its aftermath. Here $\varepsilon=1.0$ and other parameters are the same as in Fig. 3.

sues concerning access to and control of confinement states. Consider the series of stills in Fig. 7, which snapshot $+v$ bifurcation diagram sections for increasing values of φ.

In the first frame, for $\varphi=0.05$, we see that a separate branch of solutions to Eq. (7), which is trapped at $(q,v)=(0,\infty)$ for $\varphi=0$, has appeared. Although it is unstable at first, and therefore physically irrelevant for very small values of φ, it does not remain so. At a singular point $0.05<\varphi<0.08$ the occurrence of a zero real eigenvalue and a pair of complex conjugate eigenvalues with zero real part signals the appearance of a degenerate Hopf bifurcation. (Eigenvalues were computed numerically.)

In the frame for $\varphi=0.08$ the new limit point s_C and Hopf bifurcation h_C have become separated. Along the branch between them, the solutions are stable. The branch of limit cycles that emanates from h_C undergoes one or more period doubling bifurcations before ending, presumably at a homoclinic (infinite period) terminus. This branch of limit cycles is quite short, and thus not very well resolved in Fig. 7 for the lower values of φ. Note also that h_A and h_B, and the branch of limit cycles linking them, have appeared on the hysteretic curve by $\varphi=0.08$.

At a metamorphic value of φ that we designate φ_{Tm} the arms of the two separate steady-state branches are exchanged at a transcritical bifurcation. We know this point is present because the defining conditions Eq. (A2) are satisfied with $\varphi\neq 0$. [In numbers $(v,q,\varphi)_{Tm}=(1.8247\ldots, 0.1468\ldots, 0.08059\ldots)$, with $\det d^2g=-0.004687\ldots$, $\det d^2g=-0.004687\ldots, g_{PP}=-0.001250\ldots$, for values of the other parameters as given in Fig. 3. Note that the value of ε is irrelevant for calculating steady-state bifurcations such as the pitchfork and transcritical but *not* for Hopf bifurcations [15].]

After the exchange, in the frames for $\varphi=0.085$ and $\varphi=0.1$, we see the unusual occurrence of *three* Hopf bifurcations on the same branch, although this situation could be inferred from the shallow but distinct minimum and the maximum in the locus of Hopf bifurcations in Fig. 6.

The last frame of Fig. 7, for $\varphi=0.11$, is taken after h_C and h_A have collided and annihilated each other at a singular point associated with two zero eigenvalues. This is what the minimum in the curve of Hopf bifurcations means. The branch of limit cycles emanating from h_B now continues to the (presumed) homoclinic terminus. There are a couple of period doublings on it (not shown). We also see that the limit cycles are extinguished and a quiescent H mode is achieved at h_B.

Turning our attention to the L-mode branch in the last frame of Fig. 7, we see that as q is tuned past s_L the system must jump to another stable attractor. This transition is *very* different from the intrinsically hysteretic transition depicted in Fig. 3. Here the stable attractor on the H-mode branch is a limit cycle rather than a fixed point. Furthermore, this transition is *not* hysteretic. In fact, hysteresis is (locally) forbidden by the condition $g_{PP}\neq 0$ of Eq. (A2). Therefore it is not modulated by dissipation in the same way as the transition in Fig. 3, although the feedback itself is still due to nonlinear dissipation rates.

As the value of φ is increased even further, bifurcation diagrams that one could plot gradually become less meaningful. This is because $\varphi=$ constant is a first approximation, valid for small φ, to a nonlinear function $\varphi(\zeta)$, where ζ may include dynamical variables and parameters.

The type of transition shown in the last frame of Fig. 7 could serve as a model for the dithering or L-H-L transitions, followed by a quiescent H mode, that have been reported in many machines. Although there may be other mechanisms for dithering transitions—another possible scenario is given at the end of Sec. V and indicated in Fig. 6, where an oscillatory transition may occur in a very poorly dissipative system—we have at least a preliminary semiological and classification guide: if your transition is oscillatory and nonhysteretic then perhaps you should look for a strong shear flow source, if it is strongly hysteretic perhaps you should look at dissipation mechanisms. Some experimental evidence supports the idea that dithering transitions result from a strong shear-flow source. In Ref. [40], an analysis of time series data around the L-H transition in COMPASS-D suggested that a homoclinic orbit is involved in the change of stability at the transition. In stellarator W7-AS typically the quiescent ELM-free H mode is obtained after a phase characterized by quasiperiodic ELMs [41,42]. In H1 stellarator a transition to fluctuating H mode occurs at lower gas filling pressures and lower magnetic fields than the transition to quiescent H mode [43].

In terms of the governor in Fig. 1 a shear flow that is generated internally and driven externally at comparable rates is likely to give rise to interesting nonlinear dynamics, because more kinetic energy in the shear flow leads to more turbulence suppression through decorrelation, but also a larger damping effect, which then alters the competitive distribution of energy from the pressure gradient.

VII. SUMMARY AND CONCLUSION

In summary, this reduced dynamical model, comprised simply of energy input, exchange, and loss rates, reflects generic characteristics of confined plasma bulk dynamics that have not been reflected in previous models. The bifurcation and stability analysis also reveals two qualitatively different transitions. The hysteretic transition is controlled by the damping rate coefficients. The nonhysteretic transition occurs when there is a relatively strong shear-flow drive.

Symmetry breaking in this system has two major effects. Firstly, a nonzero shear-flow drive is physically inevitable, even in the best-controlled experiments, and it determines a preferred direction for the shear flow. Secondly, it interacts with the internal generation and loss dynamics to cause the metamorphosis shown in Fig. 7.

More generally, the information obtained from this analysis strengthens the thesis developed in [17]: that remarkably low-dimensional models can capture and help explain essential aspects of turbulent flows that elude understanding from numerical simulations that include resolved spatial scales, and that physical deductions can be made from observations of bifurcations.

ACKNOWLEDGMENTS

We thank J. Frederiksen for bringing to our attention the barotropic governor in Ref. [19]. R.B. would like to thank the Australian Research Council for financial support.

APPENDIX

Reduced MHD fluid equations in tokamak and stellarator geometries were originally derived by Strauss [20,21]. In the electrostatic approximation, a damped MHD fluid may be described by the following momentum and pressure convection equations:

$$\rho\frac{d\mathbf{v}}{dt}=-\nabla p+\mathbf{J}\times\mathbf{B}+\mu\nabla_{\perp}^{2}\mathbf{v}+\Omega'\tilde{p}\hat{x}-\rho\nu[\mathbf{v}-V(x)\hat{y}], \tag{A1}$$

$$\frac{dp}{dt}=\chi\nabla_{\perp}^{2}p, \tag{A2}$$

where $d/dt=\partial/\partial t+\mathbf{v}\cdot\nabla$, together with the incompressibility condition $\nabla\cdot\mathbf{v}=0$ and the resistive Ohm's law $\mathbf{E}+\mathbf{v}\times\mathbf{B}=\eta\mathbf{J}$. The symbols and notation are explained in Table I. The curl of Eq. (A1) yields a vorticity equation, which is sometimes preferred in two-dimensional fluid dynamics, but we have used the momentum form because it is more transparent physically and has a simpler correspondence to the kinetic energy. An infinite slab configuration is used for simplicity and generality, as was also assumed in Ref. [44] for a drift-kinetic treatment of plasma relaxation. It is sketched in Fig. 8, where the region $-\delta<x<\delta$ can be taken to represent a region at the edge or within a confined plasma where a transport barrier evolves.

The last term on the right hand side of Eq. (A1) removes the nonlinear shear-flow reversal symmetry of the system under $v_x(x,y,t)\rightarrow v_x(x,-y,t)$, $v_y(x,y,t)\rightarrow -v_y(x,-y,t)$, $\tilde{p}(x,y,t)\rightarrow\tilde{p}(x,-y,t)$, $V(x)\rightarrow V(x)$. Similar equations, without the symmetry-breaking term in the momentum balance, have been used by several authors [45,46,23,47,7] as a basis for studying resistive turbulence–flow interactions. The symmetry-breaking term was introduced in Ref. [23], but only *a posteriori* as an adjunct in an equation for the background poloidal flow. Here we introduce it at the outset. It models the friction force acting between the single-fluid plasma velocity $\mathbf{v}$ and an assumed external poloidal flow $V\hat{y}$. Although $V\hat{y}$ may be described for convenience as an external velocity, the term represents any asymmetric shear-inducing mechanism, such as friction with neutrals, nonambipolar ion orbit losses, or neoclassical effects not included in the slab model.

The symmetry operation on $v_0(x)\equiv\langle v_y\rangle(x)$ and $V(x)$ is sketched in Fig. 9. We are working in the frame in which there is no electrostatic potential difference across the slab. That is, it is assumed that we have made a Galilean transfor-

TABLE I. Glossary of symbols, terms, and notation.

$\mathbf{v}=\frac{1}{B_0}\hat{\mathbf{z}}\times\nabla\phi=\mathbf{v}_0+\tilde{\mathbf{v}}$	$\mathbf{E}\times\mathbf{B}$ flow velocity
$\mathbf{v}_0=\langle\mathbf{v}\rangle$	Average background component
$\tilde{\mathbf{v}}$	Fluctuating or turbulent component
$p=p_0+\tilde{p}$	Plasma pressure
$p_0=\langle p\rangle$	Average background component
$\tilde{p}$	Fluctuating or turbulent component
ρ	Average mass density of ions, assumed constant
μ	Ion viscosity coefficient
B_0	Magnetic field along the z axis
η	Resistivity
ν	Frictional damping coefficient
$\Omega'\equiv d\Omega/dx>0$	Average field line curvature, assumed constant
$\nabla_{\perp}^2$	$\partial_x^2+\partial_y^2$
$\nabla_{\parallel}$	$\partial_z+\frac{x}{L_s}\partial_y$
χ	Cross-field thermal transport coefficient
V	External flow
$\langle\cdots\rangle$	Average on (y,z) plane

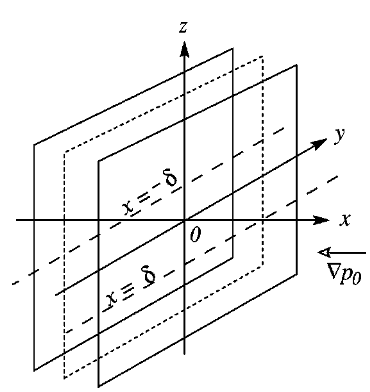

FIG. 8. Simple slab geometry is assumed. The plasma edge region is $-\delta<x<\delta$, with $x=\delta$ at the plasma surface. $\nabla p_0<0$ is the y,z-averaged pressure gradient.

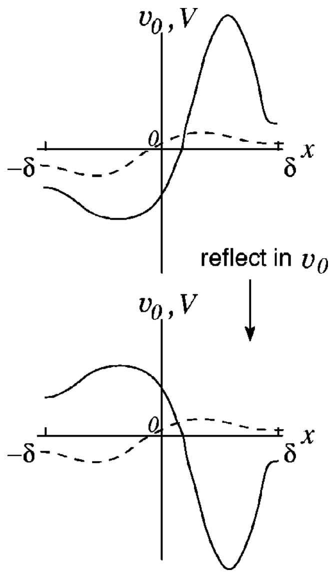

FIG. 9. Without the friction force the system is invariant under the transformation $v_0(x,t) \to -v_0(x,t)$ (solid line), $V(x) \to V(x)$ (dashed line). When the friction coefficient is $\nu \neq 0$ the symmetry is broken.

mation to the frame in which the spatial average of v_0 across the slab is zero. For simplicity we also assume that the spatial average of V is zero.

Equations (A1) and (A2) are not intended to express a detailed fluid description of a plasma, but are intended instead to represent a qualitatively authentic, semiempirical model for the essential generation and loss processes that give rise to the turbulence–shear-flow interactions that we have schematized in Fig. 1 as the plasma turbulence governor. The dynamical system Eqs. (1)–(3) can be derived from Eqs. (A1) and (A2), following the spatial averaging procedure implicit in Ref. [7].

First of all, the dynamics of the mean flow $v_0 = \langle v_y \rangle$ are extracted from the first moment $(v_y \hat{y})$ of $\langle$ Eq. (A1) $\rangle$ as

$$\partial_t v_0 - \mu \partial_x^2 v_0 + \partial_x \langle \tilde{v}_x \tilde{v}_y \rangle = -\nu(v_0 - V), \tag{A3}$$

the energy moment of which gives the spatially averaged evolution of shear flow kinetic energy F,

$$\frac{d}{dt}\left[\frac{1}{\delta}\int_{-\delta}^{\delta}\frac{dx}{2}v_0^2\right] = -\frac{1}{\delta}\int_{-\delta}^{\delta}dx\left[\mu\left(\frac{dv_0}{dx}\right)^2 + \nu v_0^2\right] + \frac{1}{\delta}\int_{-\delta}^{\delta}dx\langle \tilde{v}_x\tilde{v}_y\rangle\frac{dv_0}{dx} + \frac{1}{\delta}\int_{-\delta}^{\delta}dx\,\nu V v_0. \tag{A4}$$

This may be written as

$$\frac{dF}{dt} = -\epsilon_F + E_F + E_\varphi, \tag{A5}$$

where the definitions of ϵ_F, E_F, and E_φ correspond, respectively, to each term on the right hand side of Eq. (A4) and $F \equiv (1/\delta)\int_{-\delta}^{\delta}(dx/2)v_0^2$.

Next, the second moment of Eq. (A1) gives the total rate of evolution of F and turbulent kinetic energy N,

$$\frac{d}{dt}\left[\frac{1}{\delta}\int_{-\delta}^{\delta}\frac{dx}{2}(v_0^2 + \tilde{v}^2)\right] = \frac{1}{\delta}\int_{-\delta}^{\delta}dx\,\Omega'\frac{\langle \tilde{p}\tilde{v}_x\rangle}{\rho} - \frac{1}{\delta}\int_{-\delta}^{\delta}dx\left[\frac{\eta}{\rho_m}\langle \tilde{J}_\parallel^2\rangle + \mu\left\langle\left(\frac{\partial \tilde{v}_i}{\partial x_j}\right)^2\right\rangle\right] - \frac{1}{\delta}\int_{-\delta}^{\delta}dx\left[\mu\left(\frac{dv_0}{dx}\right)^2 + \nu v_0^2\right] + \frac{1}{\delta}\int_{-\delta}^{\delta}dx\,\nu V v_0, \tag{A6}$$

which may be expressed succinctly as

$$\frac{d}{dt}[F+N] = E_N - \epsilon_N - \epsilon_F + E_\varphi, \tag{A7}$$

where E_N and ϵ_N are defined by the first two terms on the right hand side of Eq. (A6) and $N \equiv (1/\delta)\int_{-\delta}^{\delta}(dx/2)\tilde{v}^2$.

Finally, the evolution of potential energy in the pressure gradient is defined from the x moment of Eq. (A2), assuming the cross-field thermal transport $\chi \nabla_\perp^2$ can be neglected,

$$\frac{d}{dt}\left[\frac{1}{\delta}\int_{-\delta}^{\delta}dx(-x)\Omega'\frac{p_0}{\rho}\right] = \frac{\langle \tilde{p}\tilde{v}_x\rangle|_{-\delta}^{\delta}}{\rho}\Omega' - \frac{1}{\delta}\int_{-\delta}^{\delta}dx\frac{\langle \tilde{p}\tilde{v}_x\rangle}{\rho}\Omega', \tag{A8}$$

or

$$\frac{dP}{dt} = E_P - E_N, \tag{A9}$$

with the input rate E_P defined as the first term on the right hand side and $P \equiv (1/\delta)\int_{-\delta}^{\delta}dx(-x)\Omega' p_0/\rho$.

The spatially averaged dynamical system thus consists of Eqs. (A7), (A5), and (A9). For closure we follow [7], using the approximations $p_0(x) \simeq p_0(x=\delta) + x\,dp_0/dx$ and $v_0(x) \simeq v_0(x=\delta) + x\,dv_0/dx$ for the background pressure and flow profiles and redefining P and F as the gradient terms alone. Approximations or expressions based on empirical arguments were given in Ref. [7] for the rates in Eqs. (A5), (A7), and (A9). The rates given in Eqs. (1)–(3) are economized versions of those expressions, in the sense that simpler power laws were chosen if this did not result in any qualitative changes to the singularity and stability structure of the system. The rationale is that for most of the rates we shall only learn from experiments whether different powers apply, meanwhile simple power laws give more transparent algebra.

We approximate the energy transfer rate from the pressure gradient simply as $E_N \simeq (\gamma/\varepsilon) PN$, and the energy transfer rate between the turbulence and the shear flow, due to the Reynolds stress, as $E_F \simeq \alpha FN$. The power input through the boundary is defined as $E_p \equiv q/\varepsilon$. The two-timing coefficient ε is related to the thermal capacitance, and regulates the contribution of the pressure gradient to the dynamics. For the dissipative terms we take the turbulent energy dissipation rate as $\epsilon_N \simeq \beta N^2$ and the shear-flow energy damping rate as $\epsilon_F \simeq \mu(P,N)F$, assuming the viscous damping to be dominant in ϵ_F. The external shear-flow driving rate is then $E_\varphi \simeq \varphi F^{1/2}$, with $\varphi \simeq \delta \nu V$. To obtain the evolution of the shear flow in terms of a velocity variable we redefine $v \equiv \pm F^{1/2}$. Equations (1)–(3) ensue.

A note on units: Since the emphasis in bifurcation analysis is on qualitative structure rather than numbers and unit dimensions, we have chosen to present all diagrams without the units associated with the quantities plotted. Within the lights of bifurcation theory the numbers on the axes have more value as relative measures than as absolute measurements. However, the units are easily deduced if required, from the momentum and pressure convection equations A1 and A2. Thus, for example, t is in s, P, and N are in massless energy units, $(\mathrm{m/s})^2$, v is in m/s, and q is in $\mathrm{m}^2/\mathrm{s}^3$.

[1] P. W. Terry, Rev. Mod. Phys. **72**, 109 (2000).
[2] S.-I. Itoh and K. Itoh, Phys. Rev. Lett. **60**, 2276 (1988).
[3] F. L. Hinton, Phys. Fluids B **3**, 696 (1991).
[4] P. H. Diamond, Y. M. Liang, B. A. Carreras, and P. W. Terry, Phys. Rev. Lett. **72**, 2565 (1994).
[5] O. Pogutse, W. Kerner, V. Gribkov, S. Bazdenkov, and M. Ossipenko, Plasma Phys. Controlled Fusion **36**, 1963 (1994).
[6] I. A. Vojtsekhovich, A. Y. Dnestrovskij, and V. V. Parail, Nucl. Fusion **35**, 631 (1995).
[7] H. Sugama and W. Horton, Plasma Phys. Controlled Fusion **37**, 345 (1995).
[8] V. B. Lebedev, P. H. Diamond, I. Gruzinova, and B. A. Carreras, Phys. Plasmas **2**, 3345 (1995).
[9] J. F. Drake, Y. T. Lau, P. N. Guzdar, A. B. Hassam, S. V. Novakovski, B. Rogers, and A. Zeiler, Phys. Rev. Lett. **77**, 494 (1996).
[10] G. Hu and W. Horton, Phys. Plasmas **4**, 3262 (1997).
[11] A. Takayama, T. Unemura, and M. Wakatani, Plasma Phys. Controlled Fusion **40**, 775 (1998).
[12] S.-I. Itoh, S. Toda, M. Yagi, K. Itoh, and A. Fukuyama, Plasma Phys. Controlled Fusion **40**, 737 (1998).
[13] G. M. Staebler, Nucl. Fusion **39**, 815 (1999).
[14] A. Thyagaraja, F. A. Haas, and D. J. Harvey, Phys. Plasmas **6**, 2380 (1999).
[15] R. Ball and R. L. Dewar, J. Plasma Fusion Res. **4**, 266 (2001).
[16] M. Golubitsky and D. G. Schaeffer, *Singularities and Groups in Bifurcation Theory* (Springer-Verlag, New York, 1985), Vol. 1.
[17] P. Holmes, J. L. Lumley, and G. Berkooz, *Turbulence, Coherent Structures, Dynamical Systems and Symmetry* (Cambridge University Press, Cambridge, 1996).
[18] R. Ball and R. L. Dewar, Phys. Rev. Lett. **84**, 3077 (2000).
[19] I. N. James, J. Atmos. Sci. **44**, 3710 (1987).
[20] H. R. Strauss, Phys. Fluids **20**, 1354 (1977).
[21] H. R. Strauss, Phys. Fluids **22**, 733 (1980).
[22] S. I. Braginskii, in *Reviews of Plasma Physics*, edited by M. A. Leontovich (Consultants Bureau, New York, 1965), Vol. 1.
[23] H. Sugama and W. Horton, Phys. Plasmas **1**, 345 (1994).
[24] K. Ida, S. Hidekuma, Y. Miura, T. Fujita, M. Mori, K. Hoshino, N. Suzuki, T. Yamauchi, and JFT-2M Group, Phys. Rev. Lett. **65**, 1364 (1990).
[25] D. Thomas, R. Groebner, K. Burrell, T. Osborne, and T. Carlstrom, Plasma Phys. Controlled Fusion **40**, 707 (1998).
[26] Y. Igitkhanov *et al.*, Plasma Phys. Controlled Fusion **40**, 837 (1998).
[27] M. G. Shats, Plasma Phys. Controlled Fusion **41**, 1357 (1999).
[28] P. E. Bak, N. Asakura, Y. Miura, T. Nakano, and R. Yoshino, Phys. Plasmas **8**, 1248 (2001).
[29] J. W. Connor, Plasma Phys. Controlled Fusion **40**, 531 (1998).
[30] W. Suttrop, Plasma Phys. Controlled Fusion **42**, A1 (2000).
[31] K. H. Burrell *et al.*, Phys. Plasmas **8**, 2153 (2001).
[32] R. E. Bell, F. M. Levinton, S. H. Batha, E. J. Synakowski, and M. C. Zarnstorff, Phys. Rev. Lett. **81**, 1429 (1998).
[33] W. Solomon (private communication).
[34] H. Zohm, W. Suttrop, K. Buchl, H. J. deBlank, O. Gruber, A. Kallenbach, V. Mertens, F. Ryter, and M. Schittenhelm, Plasma Phys. Controlled Fusion **37**, 437 (1995).
[35] F. Ryter *et al.*, Plasma Phys. Controlled Fusion **40**, 725 (1998).
[36] A. E. Hubbard, R. L. Boivin, J. F. Drake, M. Greenwald, Y. In, J. H. Irby, B. N. Rogers, and J. A. Snipes, Plasma Phys. Controlled Fusion **40**, 689 (1998).
[37] R. A. Moyer *et al.*, Plasma Phys. Controlled Fusion **41**, 243 (1999).
[38] H. Dahi, J. N. Talmadge, and J. L. Shohet, Phys. Rev. Lett. **80**, 3976 (1998).
[39] M. G. Shats, D. L. Rudakov, R. W. Boswell, and G. G. Borg, Phys. Plasmas **4**, 3629 (1997).
[40] J. Hugill, D. S. Broomhead, and M. Barratt, in *25th EPS Conference on Controlled Fusion and Plasma Physics ECA*, edited by P. Pavio (European Physical Society, 1998); Europhys. Conf. Abstr. **22c**, 2318 (1998).
[41] M. Hirsch *et al.*, Plasma Phys. Controlled Fusion **40**, 631 (1998).
[42] M. Hirsch *et al.*, Plasma Phys. Controlled Fusion **42**, A231 (2000).
[43] M. G. Shats and D. L. Rudakov, Phys. Rev. Lett. **79**, 2690 (1997).
[44] T. H. Stix, Phys. Fluids **16**, 1260 (1973).
[45] B. A. Carreras, L. Garcia, and P. H. Diamond, Phys. Fluids **30**, 1388 (1987).
[46] H. Sugama and M. Wakatani, J. Phys. Soc. Jpn. **57**, 2010 (1988).
[47] H. Sugama and W. Horton, Phys. Plasmas **1**, 2220 (1994).